EUROTHERM 69
Heat and Mass Transfer
in Solid-Liquid Phase Change Processes
June 25–27, 2003, Bistra castle, Ljubljana, Slovenia
Eds.: B. Šarler, D. Gobin

Experimental Results on Solidification of Aqueous Solutions of NH_4Cl

Renato Santulli, Gian Paolo Beretta, Adriano M. Lezzi*

Dipartimento di Ingegneria Meccanica
Università degli Studi di Brescia, via Branze 38, 25123, Brescia, Italy
e-mail: lezzi@ing.unibs.it

Key words: solidification, ammonium chloride, slurry zone, single-continuum approach, hybrid models

Abstract
Aqueous salt solutions are used in solidification studies as semi-transparent analog systems of metal alloys. Here, we describe an experimental apparatus to investigate solidification of NH_4Cl-H_2O solutions that has been built with the medium-term goal of collecting data for numerical codes validation and for assessment of macroscopic models of the two-phase solid-liquid zone.
Results of a preliminary set of experiments, aimed at exploring the range of solidification conditions reproducible in the apparatus, are presented and discussed. Experiments are on horizontal directional solidification between two vertical, parallel walls mantained at different temperatures. Starting with the solution at uniform ambient temperature, each experiment is continued until steady state is obtained. Different solute concentrations (6.67%, eutectic, 22%, 24%, 30%) and thermal boundary conditions are tested.
During the experiments both a mushy (dendritic matrix filled with liquid) and a slurry (solid fragments floating in liquid) zones are observed, however transition between the two zones seems to depend on more parameters than liquid fraction only, as it is usually assumed in so-called hybrid models of the two-phase zone.
Numerical simulations of the experiments are carried out with the CFD code Fluent. Computations, based on the single-continuum approach, are performed using both the porous model and a hybrid model. Comparison with experimental temperature data show that, when a slurry region is indeed present, the hybrid model performs better than the porous one.

1 Introduction

The technological quest for high quality products increases the steelmaking and foundry industry expectation of a better understanding and control of solidification. In the production of large size mechanical parts, e.g. by forging steel ingots, solidification is a critical stage because it may determine defects, as contraction porosities and macrosegregation of solutes, which cannot be eliminated in subsequent treatments and may result in the rejection of the final products. The industrial demand for an enhanced control on casting has stimulated in the last two decades fundamental and applied studies on solidification of metal alloys, especially about the effect of melt convection on solidification microstructure. Since the first fundamental theoretical and numerical studies [1, 2], several authors have tried to improve solid-liquid phase-change models. Nowadays commercial codes developed for metallurgical applications and some CFD packages enable to perform simulations of solidification in complex geometries. Unfortunately, none of these codes simulates correctly all aspects of the problem.

Phase change from liquid to solid for metal alloys takes place over a finite temperature interval that ranges between the solidus temperature T_{sol} and the liquidus temperature T_{liq}. Within this range solid structures coexist in equilibrium with liquid: the typical morphology in industrial processes is dendritic. Most of numerical simulations are not concerned with a pointwise description of the dendritic structure — its length scale is quite small, $O(10^{-5})$–$O(10^{-4})$ m — but rely on macroscopic models of it which describe the solidifying material by means of effective properties. Commercial packages, as well as many codes developed for scientific purposes, are based on the single-continuum approach: the solid phase is represented as a porous medium filled with the liquid phase. Porosity of the medium coincides with liquid fraction, therefore porosity values equal to 0 and 1 characterize the all solid and the all liquid regions, respectively. These two regions are separated by a layer, the so called mushy region, which corresponds to the growing dendritic matrix and where porosity ranges between zero and one.

Fragments can detach from dendrites. When there are significant convective motions in the melt, arms of the protruding dendrites can be broken by shear forces exerted by the flowing melt. In addition to fragmentation, arms can be released due to a “pinch off” mechanism which involves remelting at the arm base. In those cases characterized by a significant fragmentation, a description of the solidifying material as a suspension of solid particles in a liquid, at least at liquid fraction values close to one, can be more accurate than the porous medium model.

In [3, 4] a macroscopic model that takes into account the presence of fragments, was proposed. In this macroscopic model, denoted as *Mixed* model, the two-phase solid-liquid region is modeled as made of two adjacent zones: the dendritic matrix, here referred to as *mushy*, described through the porous medium approach, and a *slurry* zone characterized by the presence of solid fragments carried by the liquid. Momentum exchange between the two phases in the slurry is accounted for through an effective viscosity formulation valid for noncolloidal suspensions. Transition between the two zones is set at a fixed threshold value of liquid fraction. Very recently, Ref. [5] has brought to our attention that a substantially identical model had been proposed by Oldenburg and Spera — two researchers in the field of geological sciences — in 1992 [6]. A few years later, Ilegbusi and Mat [7] proposed another hybrid model that represents the slurry as a power-law fluid.

The *Mixed* model was implemented in CFD packages (Fluent and ProCast) to simulate solidification of steel in ingot casting and numerical results compared with experimental data collected in a steel-making plant [8]. Because of the large number of factors which govern or affect solidification in industrial casting coupled to limitations of available versions of the packages — e.g. computation of the solute concentration field could not be handled by the codes — comparison did not provide an effective criterion to assess improvement in the two-phase region description due to the *Mixed* model. To bypass these difficulties in

validation of the *Mixed* versus the porous model, attention has been focused on solidification problems simpler than ingot casting: crystallization of aqueous solutions of ammonium chloride in a rectangular cavity. For this purpose our group has undertaken the construction of the experimental apparatus, described in this paper, and the development of a finite element code that has not been completed yet.
Aqueous salt solutions have been and are still extensively used as model systems to investigate solidification [9]. As metal alloys, these mixtures exhibit a dendritic morphology during solidification, however they have the advantage of being semi-transparent, thus allowing the use of optical techniques to visualize flow patterns and to track solidus and liquidus fronts. Besides, they are characterized by low melting temperatures which are more easily controlled in a laboratory then typical melting ranges of metal. Although results obtained for these model systems cannot be extended automatically to metal alloy solidification because of the different order of magnitude of many thermophysical properties, nevertheless they have yielded elucidation of many mechanisms at work during solidification. In addition, aqueous salt solutions are important as they allow to set-up experiments and collect data for validation of numerical codes, which is the motivation for the work reported in this paper.
In Sec. 2 we describe the experimental apparatus built to visualize solidification of NH_4Cl-H_2O. The experimental procedure, the parameters that characterize each experimental run, as well as a qualitative description of the solidification patterns observed, are presented in Sec. 3. In Sec. 4 numerical simulations of three visualization experiments are briefly reviewed. Although the experimental and numerical activities performed until now have to be considered just as preliminary, in Sec. 5 a few remarks on the criterion for transition between mushy and slurry zones in hybrid models are discussed.

2 Experimental apparatus

Fig. 1 shows a schematic drawing of the experimental apparatus, which is made of the test section, two constant temperature baths and a data acquisistion system for temperature measurements.
The test section, or solidification cell, is a rectangular box made of four plexiglas walls (front, rear, top and bottom) and two aluminum alloy sidewalls. The cavity bounded by the cell walls is 72 mm wide, 150 mm high and 110 mm deep. An inlet port in the top wall and an outlet port in the bottom wall allow to fill and empty the cell.
Thermal control over the cell is ensured through the sidewalls that act as heat exchangers. Each of them is an aluminum alloy plate 47 mm thick, 160 mm high and 122 mm deep. A working fluid circulate through the plate to regulate its temperature. The cold plate is chilled by alcohol cooled in a cryostat (Haake, Phoenix P1-C50P). Water from a thermostat (Haake, Phoenix P1-B7) flows through the hot plate; water temperature lower than 20°C can be obtained letting the alcohol flow through a serpentine immersed in the P1-B7 bath.
During the experiments the cell is placed inside a box made of 50 mm thick expanded polystyrene slab. Cavities and gaps between the cell and the polystyrene case are filled with fiberglass. The polystyrene block that covers the front wall can be removed easily to take photographs of the solidification process.
The rear wall is fitted with a two-dimensional array (14 rows by 7 columns) of 98 thermocouple ports for temperature measurements within the solidifying medium. The pitch between adjacent rows and columns is 10 mm.
Temperature measurements are made with K-type stainless steel sheathed, 1.6 mm O.D. thermocouples. During the experiments 31 thermocouples are usually used — their tip locations are shown in Fig. 3(a). Each thermocouple is inserted in the cell up to a distance of 60 mm from the internal surface of the rear wall. Uncertainties in the thermocouple tip locations are estimated to be within ± 1 mm in x, y,

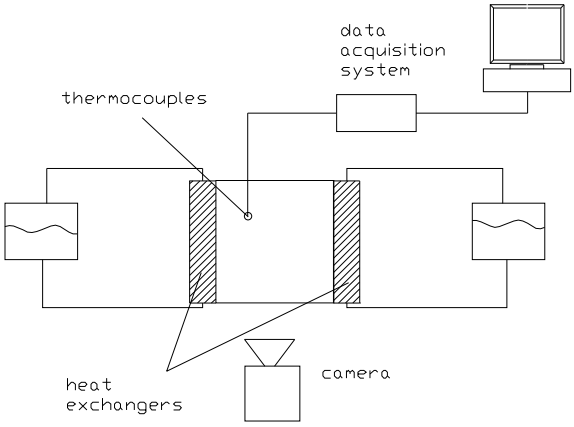

Figure 1: Schematic of the experimental apparatus.

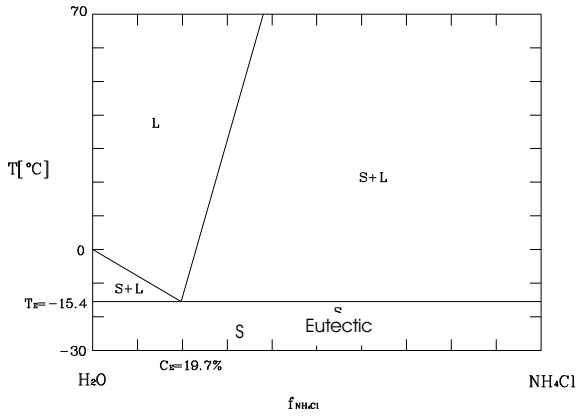

Figure 2: Equilibrium phase diagram of NH_4Cl-H_2O system.

and z directions. Six additional thermocouples are inserted in the two aluminum plates to control their temperature during the experiments.
Thermocouple calibration has been carried out with care, using the constant temperature baths and a calibrated four-lead platinum resistance PT100 as reference thermometer. The estimated accuracy of the calibrated TCs is within ± 0.15 K.

3 Experimental results

In the visualization experiments reported in this paper aqueous solutions of ammonium chloride have been used as solidifyng material. The equilibrium phase diagram for NH_4Cl–H_2O is shown in Fig. 2.
Eutectic composition is characterized by NH_4Cl mass fraction $f_{\rm e}^{\rm NH_4Cl} = 19.7\%$ and eutectic temperature $T_{\rm e} = -15.4$°C. The liquidus temperature is strongly dependent on NH_4Cl concentration, both for hypoeutectic and hypereutectic compositions, whereas the solidus lines are vertical, thus $T_{\rm sol}$ is identically equal to $T_{\rm e}$.
In the experiments solutions of five different concentrations have been tested: one hypoeutectic (6.67%), one almost eutectic (20%), and three hypereutectic (22%, 24%, 30%).
Nominal thermal boundary conditions imposed on the solution during the experiment are: uniform and constant temperature at the sidewalls—cold wall on the left, and hot wall on the right, looking at the cell front— zero heat flux on the other four walls (see Tab. 1). Starting with the solution at uniform temperature T_i, the experiment is continued until steady state is obtained. Actual experimental procedure has been the following. Circulation of alcohol and water from the constant temperature baths through the sidewall heat exchangers is started while the cell is empty. As soon as the sidewalls reach the desidered temperature, solution is introduced through the supply port at $T_i = 20$°C. It takes about 10–20 s to fill the cell. During this time lapse sidewall surface temperatures change abruptly, especially on the cold wall (up to 10°C, approximately). However the bath temperature controller which is connected to a PT100 probe, inserted in the sidewall close to its wetted surface, restores the imposed temperature within 10–15 minutes.
Output from the 37 thermocouples are read every 60 s by a data acquisition unit and sent to an on-line PC for storage and post-processing. Periodically, the polystyrene cover of the cell front wall is removed to observe and take photographs of the advancing solidification fronts.

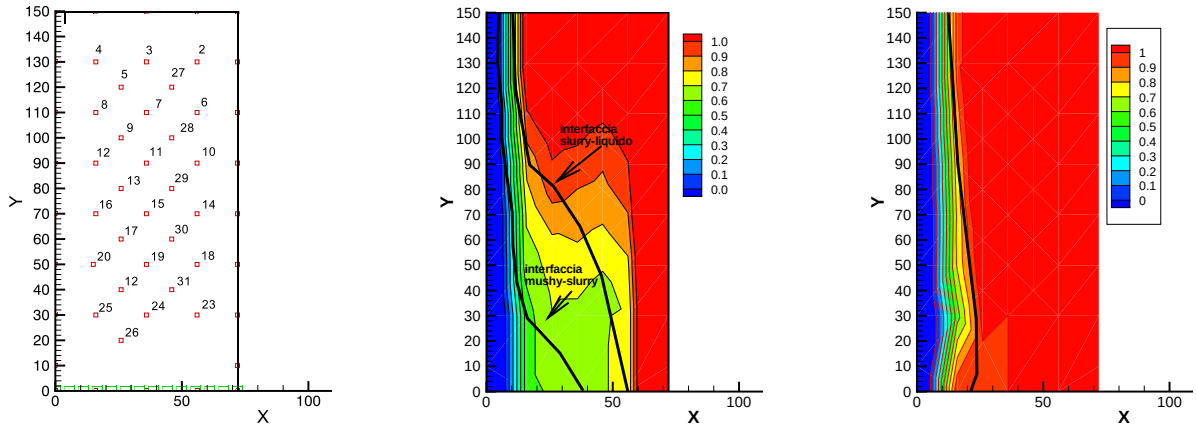

(a) (b) (c)

Figure 3: (a) Locations of thermocouple tips in the vertical, front plane. The outer rectangle represents the perimeter wetted by the solution. (b), (c) Non-dimensional temperature field θ, obtained upon interpolation of experimental data. Solid lines represent interfaces between different zones. Their positions have been determined by photographs. (b): $f^{\mathrm{NH_4Cl}} = 22\%$, $T_c = -20$°C, $T_h = 5$°C, at $t = 3000$ s; (c): $f^{\mathrm{NH_4Cl}} = 6.67\%$, $T_c = -20$°C, $T_h = 5$°C, at steady state.

Instantaneous temperature field is obtained upon bilinear interpolation of data from TCs in the cell and in the sidewalls, imposing zero temperature normal derivative at the top and bottom walls. Solid-mushy, mushy-liquid or mushy-slurry, and slurry-liquid interface positions, as surveyed from available photographs, are drawn on the temperature field (see, e.g. Fig. 3(b) and (c)). To facilitate comparison, temperature is plotted in the following non-dimensional form:

$$\theta = \frac{T - T_{\mathrm{sol}}}{T_{\mathrm{liq}} - T_{\mathrm{sol}}}, \quad \text{for } T_{\mathrm{sol}} \leq T \leq T_{\mathrm{liq}} \tag{1}$$

for $T < T_{\mathrm{sol}}$ and $T_{\mathrm{liq}} < T$, θ is set equal to 0 and 1, respectively. Here, T_{liq} is the liquidus temperature at the solution nominal concentration. As solidification progresses, solute concentration in the remaining liquid changes, tending to $f_{\mathrm{e}}^{\mathrm{NH_4Cl}}$. Under the rather crude approximation of uniform and constant con-

Table 1: Nominal thermal boundary conditions and initial concentrations. X denotes a condition tested, whereas N indicates that numerical simulation of the experiment has been carried out.

T_c / [°C]	T_h / [°C]	NH_4Cl concentration / [wt%] liquidus temperature / [°C]				
		6.67% -5	20% T_{e}	22% -5	24% 5	30% 35
-25	40					X
-25	35				X	
-25	20		X		X-N	X
-15	20		X		X	
-25	10		X		X	
-20	5	X-N		X-N		

centration, the variable θ coincides with the liquid fraction f_l.
In Fig. 4 representative pictures of what observed in the experiment are shown. Figs. 4(a), (b), and (c), are taken at about 240, 1100, and 2800 s since filling the cell with a 24wt% NH_4Cl, for nominal side-wall temperatures T_c and T_h equal to -20 and 30°C, respectively. Anticlockwise circulation induced by the imposed temperature difference across the cell quickly develops. During the first minutes, though, neither a mushy or solid layer can be clearly recognized over the chilled wall. Dendrites that develop at some nucleation sites are soon torn by shear forces exerted by the descending cold liquid layer. These salt crystals are heavier than surrounding liquid and tend to move towards the bottom of the cell. In Fig. 4(a) it is evident the presence of a slurry, characterized by a foggy appearance, in the bottom left corner of the cell. Here temperature is smaller than T_{liq}, so fragments can not remelt. Successively, thin solid and mushy layers develop over the cold wall. Temperature field reaches steady state at 1500 s, approximately, whereas thickness of the solid and the mushy layers grows for a few more minutes. At the bottom, a slurry zone of slightly reduced extent seems to be still present.
Figs. 4(d), (e), and (f) refer to solidification of a 22wt% NH_4Cl solution, for cold and hot wall temperatures equal to -20 and 5°C, respectively. Photographs are taken after 30, 50 minutes and at steady state. In the pictures white zones correspond to solid NH_4Cl, milky areas indicate presence of the mush, the slurry is clearly recognized in Figs. 4(d) and (e) for the presence of floating particles. In this experiment a significant production of dendritic fragments is observed. Comparison of Fig. 4(d) with the previous ones shows that the mushy layer is thicker than in the other experiment and non uniform, increasing irregularly from top to bottom. The interface between the mush and the adjacent liquid is rough and sort of "flakes" protruding outwards can be distinguished. Besides shear induced fragmentation of dendritic tips and detachment by remelting, a third solid particle production mechanisms is active during the first part of the experiment: large "flakes" grow and detach from nucleation sites in the upper part of the cold plate. These fragments slide down towards the cell bottom, recalling an "avalanche" that drags down further solid particles. The process leads to a significant accumulation of sediment on the cell bottom that extends to a short distance from the hot plate where the increasing temperature cause remelting of the particles. A rather thick slurry zone separate the mushy zone from the pure liquid in the middle and lower part of the cold wall, as appears in both Figs. 4(d) and (e). As the system approaches steady state, a solid layer develops and thickens, the mushy zone seems to incorporate the bottom sediment and its boundary becomes more regular. Fragment production ceases and the slurry zone tends to disappear, except possibly at the right end of the sediment.
Finally, Figs. 4(g) (30 minutes) and 4(h) (steady state) refer to solidification of a hypoeutectic solution, $f^{\mathrm{NH_4Cl}} = 6.67\%$, for cold and hot wall temperatures equal to -20 and 5°C, respectively. The liquidus temperature, as well as thermal boundary and initial conditions, are the same of the previous experiment. However, thermosolutal convection effects lead to a mush growth pattern completely different. Here the solid phase is made of ice crystals and the mush develops as a layer of rather uniform thickness over the entire cold plate. Ice fragments are hardly distinguishable. Since ice has smaller density than NH_4Cl-H_2O solution, fragments have positive buoyancy and tend to rise towards warmer zones where they melt.

4 Numerical simulations

Simulations of three solidification experiments (see Tab. 1) have been carried out with the CFD package Fluent. Temperature numerical estimates have been compared with experimental data to verify whether a hybrid model might introduce effective improvements in the two-phase zone macroscopic description. Numerical analysis is based on the single-continuum approach and both the porous and the *Mixed* model

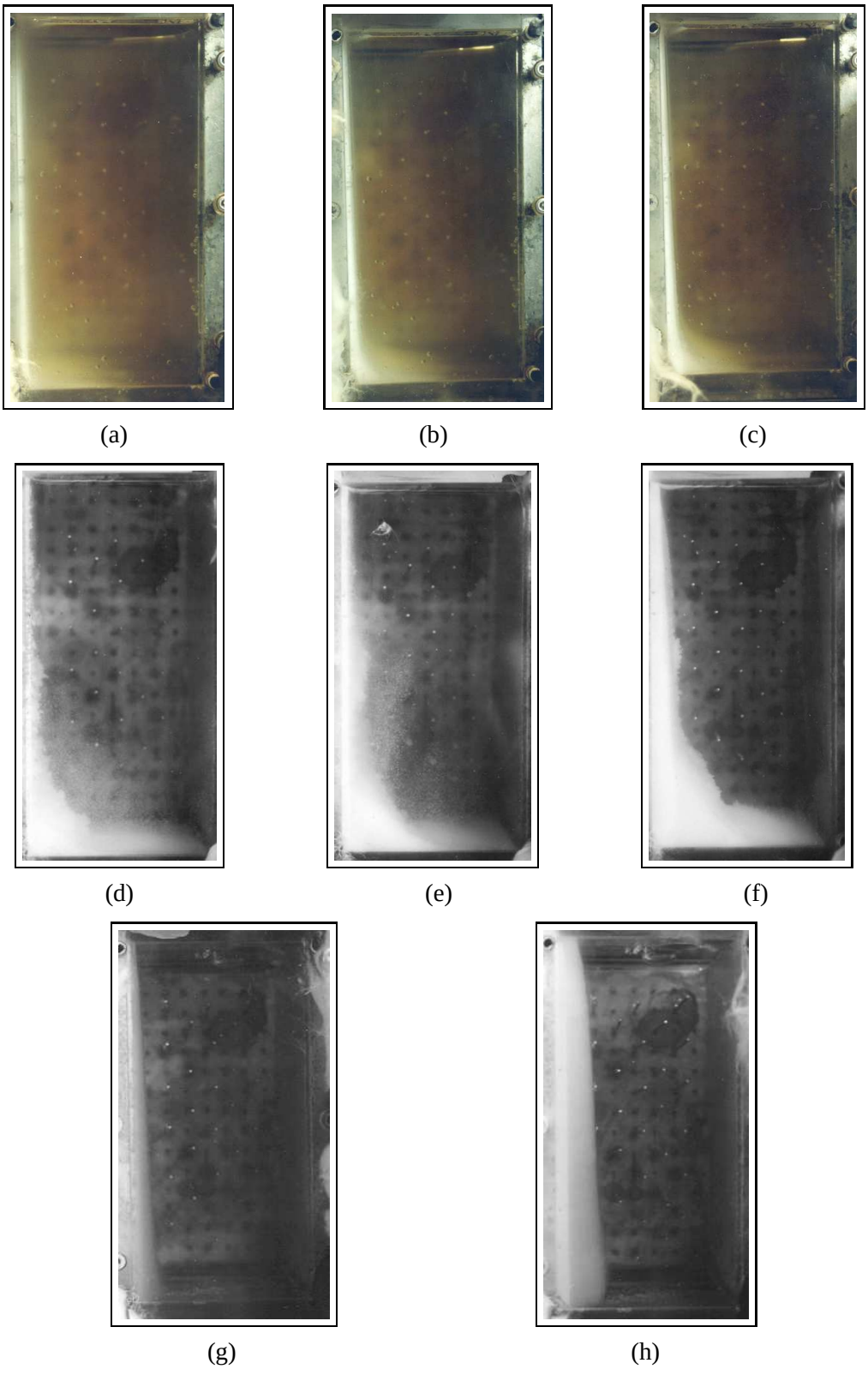

Figure 4: Photographs of the solidifying material. (a)-(c): $f^{\mathrm{NH_4Cl}} = 24\%$, $T_c = -20$°C, $T_h = 30$°C, 240 s, 1100 s, and steady state, respectively; (d)-(f): $f^{\mathrm{NH_4Cl}} = 22\%$, $T_c = -20$°C, $T_h = 5$°C, 1800 s, 3000 s, and steady state, respectively; (g)-(h): $f^{\mathrm{NH_4Cl}} = 6.67\%$, $T_c = -20$°C, $T_h = 5$°C, 1800 s and steady state, respectively.

have been used. Current version of Fluent does not allow to handle the species conservation equation in simulation of solidification problems. Thus, a constant NH_4Cl concentration has been assumed in all computations. The following additional assumptions have been taken: density ρ and specific heat c are constant and have the same value for both the solid and the liquid phases; thermal conductivity k is a volume average of the conductivity of the solid and the liquid phases; buoyancy effects are accounted for using the Boussinesq approximation; in the two-phase region the liquid fraction depends linearly on temperature and coincides with non-dimensional temperature θ defined by Eq. (1).
The equation set solved is the following,

$$\nabla \cdot \mathbf{u} = 0 \tag{2}$$

$$\frac{\partial}{\partial t}(\rho \mathbf{u}) + \nabla \cdot (\rho \mathbf{u}\mathbf{u}) = -\nabla p' + \mu_{\mathrm{e}} \nabla^2 \mathbf{u} - \rho \beta (T - T_0)\, \mathbf{g} + \mathbf{S} \tag{3}$$

$$\frac{\partial}{\partial t}(\rho H) + \nabla \cdot (\rho \mathbf{u} H) = \nabla \cdot (k \nabla T) \tag{4}$$

where p' represents the pressure without the hydrostatic contribution and T_0 is a reference temperature. In Eq. (4) the total enthalpy H is calculated as

$$H = H_{\mathrm{s\,ref}} + \int_{T_{\mathrm{ref}}}^{T} c_e \, dT \tag{5}$$

where an effective specific heat c_e is introduced to account for the gradual release of the latent heat of fusion L. c_e is equal to $c + L/(T_{\mathrm{liq}} - T_{\mathrm{sol}})$ for T between the solidus and the liquidus temperature, and coincides with c otherwise.
Key terms for modeling the two-phase region are the momentum source

$$\mathbf{S} = -\frac{\mu_{\mathrm{l}}}{K}\mathbf{u}. \tag{6}$$

and the effective viscosity

$$\mu_e = \mu_l \left[1 + \frac{1.5(1 - f_l)}{1 - ((1 - f_l)/0.58)}\right]^2 \tag{7}$$

The source term $\mathbf{S}$ is introduced to describe the flow in the mushy region as the flow in a porous medium. Here K represents the medium permeability that is calculated using the Kozeny-Carman equation

$$K = C \frac{f_l^3}{(1 - f_l)^2}. \tag{8}$$

The dendritic matrix porosity has been assumed equal to the liquid fraction. The value of the constant C, which depends on the dendritic arm spacing, has been set equal to 5.556×10^{-11} m^2 [1].
Eq. (7) expresses viscosity of a suspension of rigid noncolloidal spherical particles of uniform size in an incompressible liquid of viscosity μ_l [10].
In the porous model the source term $\mathbf{S}$ is equal to zero for $f_l = 1$, and $\mu_e = \mu_l$. In the *Mixed* model a slurry layer exists between the pure liquid and the mushy zone. Mushy-slurry interface is set at a fixed value of liquid fraction, here denoted as $f_{l,\mathrm{th}}$. Therefore, for liquid fraction values between $f_{l,\mathrm{th}}$ and 1 Eq. (7) is used and the term $\mathbf{S}$ is set equal to zero, whereas for $f_l < f_{l,\mathrm{th}}$ Eq. (7) is used and μ_e is set equal the solution viscosity μ_l.
In numerical simulations, all two-dimensional, constant temperature BCs have been imposed on the side-walls, whereas the upper and lower walls of the cell have been considered adiabatic. The solution has always been considered initially at rest, at uniform temperature $T_i = 20$ ℃, thus neglecting to model the

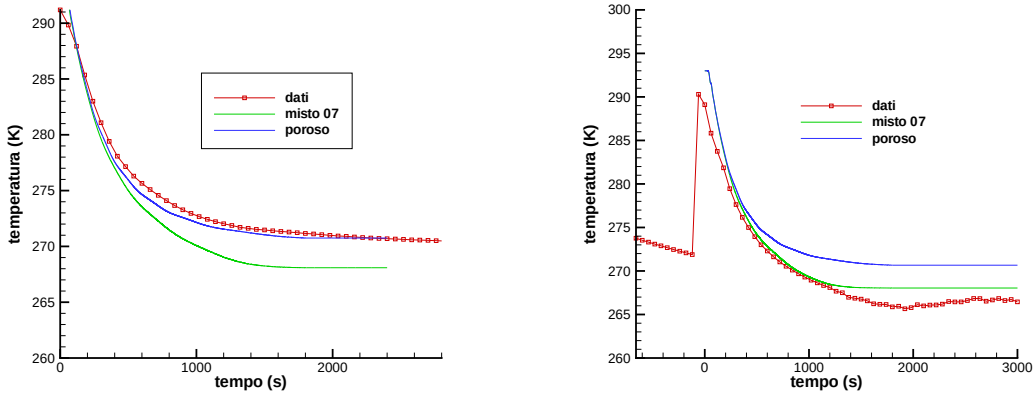

Figure 5: temperature at TC no. 15 location *vs.* time; experimental data (squares), *Mixed* model (green dashed line), porous model (blue solid line). (a): $f^{\mathrm{NH_4Cl}} = 6.67\%$, $T_c = -20$℃, $T_h = 5$℃; (b): $f^{\mathrm{NH_4Cl}} = 22\%$, $T_c = -20$℃, $T_h = 5$℃.

cell filling and the sidewalls temperature transient.
Computations with the porous model — which is currently available in Fluent — have been performed with trial version 6.0.11 of the code. For computations with the *Mixed* model, v. 5.4 of the code has been used, suitably adapted by means of user-defined functions.
Typical numerical results compared with experimental temperature data at one TC location are shown in Fig. 5. Depending on the transition value $f_{l,\mathrm{th}}$ adopted in the model, relatively large differences are observed. Although comparison of measured temperature fields with photographs has not shown a clear relation between a particular liquid fraction value and the mushy-slurry interface (see Sec. 3), computations performed with $f_{l,\mathrm{th}} = 0.7$ show that adoption of the *Mixed* model does allow a reasonable prediction of temperature when a significant amount of slurries are indeed present, as in Fig. 5(b). When fragments are not present or rapidly remelt as in the hypoeutectic case (Fig. 5(a)) the porous model performs better.

5 Discussion

The experimental apparatus described in Sec. 2 has been built with the medium-term goal of collecting experimental data for code validation and for assessment of macroscopic models for the two-phase zone. The experiments reported here constitute a first set aimed at a preliminary exploration of the range of solidification conditions reproducible in the cell, rather than a systematic investigation on specific aspects of the process. However, some remarks can be made.
The experiments confirm that the solid-liquid two-phase region that separates pure solid from liquid in solidification of the NH_4Cl-H_2O system has to be regarded as composed of two zones: a fluid-saturated dendritic matrix and a suspension of matrix fragments. The extension of the two zones depends on several parameters and, likely, on solidification hystory also. From the experimental observations, the mushy zone thickness at steady state seems to be a decreasing function of the temperature difference $T_h - T_{\mathrm{liq}}$. As a consequence, for hypereutectic solutions and constant hot wall temperature, it is an increasing function of NH_4Cl concentration. There is no evidence of a dependence on cold wall temperature.
The slurry zone extension changes during the initial transient and tends to disappear or to reduce greatly at steady state. Significant fragment populations are observed for hypereutectic solutions when hot wall

temperature is close to the liquidus temperature. In these cases, detachment and falling of dendrite lumps and fragment sedimentation cause accumulation of solid phase at the cell bottom.
The presence of slurries justifies introduction of hybrid models. Indeed, our numerical results show an improvement of the *Mixed* model versus the porous model for those cases characterized by the presence of floating fragments. This conclusion requires further confirmations, since we are aware that neglecting concentration changes and restricting comparison to temperature data only limits the significance of the comparison.
Also questionable appears the criterion adopted to define the transition between the porous medium and the effective viscosity model of the slurry. A first objection to setting transition at a fixed value of liquid fraction is that interfaces between single-phase and two-phase zones deviate substantially from isotherms, as in Fig. 3. This is a weak objection, since isotherms and iso-liquid-fraction-lines coincide only if solute concentration is assumed uniform in the solidifying material, as mentioned in Sec. 3. Based on qualitative reasoning, as $f^{\mathrm{NH_4Cl}}$ in the mush and in the liquid zones tends towards $f_{\mathrm{e}}^{\mathrm{NH_4Cl}}$, iso-liquid-fraction-lines should approach closer than isotherms to the interfaces. However, without concentration measurements no quantitative estimates can be made. A second, stronger objection is that slurries are observed mainly during the transient and for a limited set of conditions. Therefore, any criterion that assumes the presence of a slurry for liquid fractions larger than a threshold value independent of time and boundary conditions, is likely to yield inaccurate predictions.

References

[1] W. Bennon, F. Incropera, *A continuum model for momentum, heat and species transport in binary solid-liquid phase change systems — I. Model formulation — II. Application to solidification in a rectangular cavity*, Int. J. Heat Mass Transfer, 30, (1987), 2161–2187.

[2] V. Voller, C. Prakash, *A fixed grid numerical modelling methodology for convection-diffusion mushy region phase-change problems*, Int. J. Heat Mass Transfer, 30, (1987), 1709–1719.

[3] M. Pilotelli, *Numerical study of thermal-fluid dynamical models for the two-phase region in steel solidification in cavities*, Ph.D. thesis, Università degli Studi di Brescia (1999), in Italian.

[4] M. Pilotelli, R. Santulli, G. Beretta, A. Lezzi, *Natural convection effects on the solidification of a steel ingot*, in *Proc. XVIII UIT Nat. Heat Transfer Conf.*, Cernobbio (2000), pp. 383–396, in Italian.

[5] S. Chakraborty, P. Dutta, *Three-dimensional double-diffusive convection and macrosegregation during non-equilibrium solidification of binary mixtures*, Int. J. Heat Mass Transfer, 46, (2003), 2115–2134.

[6] C. Oldenburg, F. Spera, *Hybrid model for solidification and convection*, Num. Heat Transfer, 21, (1992), 217–229.

[7] O. Ilegbusi, M. Mat, *A hybrid model of mushy region in phase-change problems*, J. Mater. Process. Manuf. Sci., 5, (1997), 209–223.

[8] A. Lezzi, M. Pilotelli, R. Santulli, *Ingot and mould temperature measurements during the production of large size steel ingots*, in *Proc. 12th IHTC*, Grenoble (2002), pp. 791–796.

[9] F. Incropera, *Experimental methods for characterizing transport phenomena occurring during solidification of multiconstituent materials*, in M. Giot, F. Mayinger, G. Celata, eds., *Experimental Heat Transfer, Fluid Mechanics and Thermodynamics, 1997*, Edizioni ETS (1997), pp. 1855–1867.

[10] A. Acrivos, A. Fan, R. Mauri, *On the measurement of the relative viscosity of suspensions*, J. Rheol., 38, (1994), 1285–1296.